Available online at www.sciencedirect.com
ScienceDirect
Geochimica et Cosmochimica Acta 71 (2007) 3170–3181
Geochimica et Cosmochimica Acta
www.elsevier.com/locate/gca

Equilibrium isotopic fractionation in the kaolinite, quartz, water system: Prediction from first-principles density-functional theory

Merlin Méheut [a,*], Michele Lazzeri [a], Etienne Balan [a,b], Francesco Mauri [a]

[a] IMPMC, Université Paris VI et VII, CNRS, IPGP, 4 Place Jussieu, 75252, Paris cedex 05, France
[b] IRD—UMR CEREGE, Europole Méditerranéen de l'Arbois, BP 80, 13545 Aix en Provence cedex, France

Received 14 December 2006; accepted in revised form 2 April 2007; available online 19 April 2007

Abstract

Isotopic fractionation factors for oxygen, hydrogen and silicon have been calculated using first-principles methods for the kaolinite, quartz, water (ice and gas water) system. Good agreement between theory and experiment is obtained for mineral–water oxygen isotope fractionation. This approach gives reliable results on isotopic fractionation factors as a function of temperature, within a relative precision of typically 5%. These calculations provide independent quantitative constraints on the internal fractionation of oxygen in kaolinite, the fractionation of silicon isotopes at equilibrium, or hydrogen fractionation between kaolinite and water. Calculated fractionation factors at 300 K are 12.5‰ for the kaolinite internal-fractionation of oxygen, and 1.6‰ for silicon fractionation between quartz and kaolinite.

1. INTRODUCTION

Stable isotopes are commonly used as tracers and as paleothermometers. Isotopic paleothermometry is based on the fact that the isotopic composition of two cogenetic phases is a function of the temperature at which these phases were in equilibrium. The determination of the fractionation mechanisms and the derivation of quantitative laws is of great importance in geochemistry (Valley et al., 1986). Isotopic composition measurements on natural or synthetic systems can be used to establish quantitative relationships between the isotopic composition and the temperature of the system (Clayton, 1972; Kulla and Anderson, 1978; Kita et al., 1985; Sheppard and Gilg, 1996). However, measurements on real systems have to face the slow kinetics of isotopic exchange, making it difficult to ascertain the equilibrium state of the natural or experimental systems. The derived laws are therefore well suited for high temperature systems, whereas larger uncertainties subsist at low temperature (Clayton, 1972; James and Baker, 1976; O'Neil and Kharaka, 1976; Matsuhisa et al., 1978).

Theoretical approaches may supply to these limits by providing equilibrium fractionation laws at low temperature (Urey, 1947; Richet et al., 1977; Kawabe, 1978). In addition, they can be applied to non-conventional isotopes for which experimental calibrations are lacking. Theoretical approaches mostly consist in applying statistical thermodynamics to calculate the equilibrium constants of isotope exchange reactions from the rotational and vibrational energy levels of the reactants and products. The energy levels can be determined experimentally, i.e. from spectroscopic measurements, or theoretically from atomistic calculations, or more generally using a combination of both. Indeed, spectroscopic data are usually lacking for isotopic species containing rare isotopes. Empirical rules and force-field models have thus been developed to extrapolate the spectroscopic constants of isotopically substituted molecules from those with the natural isotopic abundance (Rosenthal, 1935; Shaffer and Schuman, 1944; Richet et al., 1977; Zeebe, 2005). Alternatively, energy levels can be fully

* Corresponding author. Fax: +331 442 73 785.
E-mail address: merlin.meheut@impmc.jussieu.fr (M. Méheut).

0016-7037/$ - see front matter © 2007 Elsevier Ltd. All rights reserved.
doi:10.1016/j.gca.2007.04.012

determined theoretically using empirical potentials or ab initio electronic structure calculations. In this last case, the energy levels are calculated using fundamental quantum mechanical theory.

For molecules in gas phase, theoretical calculations can reach a very good precision (Richet et al., 1977; Zeebe, 2005). For solids, an additional difficulty arises from the need to compute the complete vibrational density of state (VDOS) of pure and isotopically substituted compounds, whereas most of the vibrational spectroscopic experiments only provide a limited set of data. The most common approach is therefore to use a simplified model of the vibrational density of states, consisting of a Debye model for acoustic modes, optical continua for low-frequency optical modes, and an Einstein model for high-frequency optical modes (Kawabe, 1978; Kieffer, 1982). Following Patel et al. (1991) and Dove et al. (1992), an alternative scheme was based on the computer modeling of crystal structures enabling a complete calculation of the VDOS. This calculation can also be done from first-principles, within the framework of density functional perturbation theory (DFPT). Indeed, DFPT has proved to be accurate in determining harmonic phonon frequencies in crystalline solids for any wavevector (Baroni et al., 2001). DFPT has been successfully applied to the investigations of the vibrational spectroscopic properties of several minerals including quartz, zircon, kaolinite-group minerals, serpentine minerals and gibbsite (Gonze et al., 1994; Balan et al., 2001, 2002, 2006; Rignanese and Gonze, 2001). The quality of the modeling of the IR and Raman spectra of these minerals indicate that accurate vibrational density of state, and thermodynamical functions, can be derived using DFPT. Recently, this approach has been applied to isotopic fractionation between various carbonate minerals (Schauble et al., 2006).

In this paper, we use DFPT to determine the isotopic fractionation of hydrogen, oxygen and silicon in the kaolinite, quartz, water (ice and gas water) system. The goal is the validation of a purely first-principles (i.e. parameter free) approach and this will be done by studying a set of well-constrained systems. Actual calculations are done on the kaolinite, quartz and hexagonal-ice water crystals. Gas-water is simulated using an isolated H_2O molecule. The isotopic-fractionation between kaolinite/liquid-water and quartz/liquid-water are also obtained by using the experimental gas/liquid-water fractionation. The choice of these systems has been driven by several considerations. The kaolinite/water and quartz/water isotopic fractionation curves are widely used in paleothermometric or paleoclimatic reconstructions (e.g. Nordt et al., 1998; Girard et al., 2000; Alexandre et al., 2004), whereas the slow dissolution and crystallization of these phases makes it difficult to derive experimental fractionation curves at low temperature (Clayton, 1972; O'Neil and Kharaka, 1976; Matsuhisa et al., 1978). Moreover, a relatively large set of measurements and calculations of the structural, spectroscopic and isotopic properties of these systems is available. The comparison with previous experimental and theoretical investigations makes it possible to assess the accuracy of the first-principles method in this context.

2. METHOD

2.1. The isotopic fractionation factor α

The isotopic fractionation factor of an element between two phases a and b, both containing two isotopic forms Y and Y^*, is defined as the overall ratio of isotopes Y^* and Y in the phase a as compared with the same ratio in b:

$$\alpha(a,b,Y)=\frac{(n_{Y^*}/n_Y)_a}{(n_{Y^*}/n_Y)_b}, \tag{1}$$

where n_Y is the number of Y atoms. In the following, Y^* will correspond to the least abundant isotope. Following Richet et al., 1977, the β-factor is the isotopic fractionation factor of Y between the phase a and a perfect gas of Y atoms, having the natural mean isotopic concentration:

$$\beta(a,Y)=\frac{(n_{Y^*}/n_Y)_a}{(n_{Y^*}/n_Y)_{gas}}. \tag{2}$$

Therefore, $\alpha(a,b,Y)$ is given by the ratio $\beta(a,Y)/\beta(b,Y)$.

For a periodic solid in the phase a and with chemical-composition of the unit-cell AY_n, we call $\beta(a,Y_i)$ the β factor related to a specific atomic site i. $\beta(a,Y_i)$ can be calculated assuming that: (i) the mean number of atoms Y^* per unit cell is small with respect to 1 (dilute limit), (ii) the free energy on the site i does not depend on the occupation of the same site in a neighboring unit-cell. Under conditions (i) and (ii),

$$\beta(a,Y_i)=\frac{Q(AY_{n-1}Y_i^*)/Q(AY_n)}{Q_g(Y^*)/Q_g(Y)}, \tag{3}$$

$$\beta(a,Y)=\frac{1}{n}\sum_{i=1}^{n}\beta(a,Y_i), \tag{4}$$

where $Q(AY_{n-1}Y_i^*)$ is the partition function of the system having the atom Y on the site i substituted with Y^*, $Q(AY_n)$ is the partition function of the system having no substituted atoms, $Q_g(Y)$ is the partition-function of a gas of atoms Y. For a perfect gas, Q_g is reduced to its translational part:

$$Q_g(Y)=\left(\frac{2\pi m_Y kT}{h^2}\right)^{3/2}V, \tag{5}$$

where m_Y is the mass of the atom Y, k is the Boltzmann constant, T is the temperature, h the Planck constant, and V is the volume. Putting together Eqs. (3)–(5), one obtains

$$\beta(a,Y)=\left(\frac{1}{n}\sum_{i=1}^{n}\left[\frac{Q(AY_{n-1}Y_i^*)}{Q(AY_n)}\right]\right)\left[\frac{m_Y}{m_{Y^*}}\right]^{3/2}. \tag{6}$$

Eq. (6) is not the standard equation used in literature to compute β. A different equation is obtained considering two more-stringent conditions which are: (i) the free energy change associated to the isotopic substitution of an atom Y does not depend on the isotopic nature of the surrounding Y atoms, (ii) $\beta(a,Y_i)$ weakly depends on the site i in such a way that

$$\frac{1}{n}\sum_{i=1}^{n}\beta(a,Y_i)\cong\left[\prod_{i=1,n}\beta(a,Y_i)\right]^{1/n}. \tag{7}$$

Under conditions (i) and (ii),

$$\beta(a,Y) = \left[\frac{Q(AY_n^*)}{Q(AY_n)}\right]^{1/n}\left[\frac{m_Y}{m_{Y^*}}\right]^{3/2}, \quad (8)$$

where $Q(AY_n^*)$ is the partition function of the system having all the Y atoms substituted with Y^*. Eq. (8) is commonly used in literature (Richet et al., 1977 and Chacko et al., 2001). However, in some specific cases, the assumptions behind Eq. (8) are not satisfied. For example, when deuterium is substituted for hydrogen in water, the free energy change related to the substitution of the second hydrogen is very different from that of the first one. In this case, Eq. (6) is more accurate.

2.2. The partition function

For a given system, solid or gas, with accessible states (l) of energy E_l, the partition function is

$$Q = \sum_l e^{-E_l/(kT)}. \quad (9)$$

2.2.1. Gaseous compound

For a gaseous compound (perfect gas model), in the harmonic approximation, the contributions to the partition function of translational, vibrational, and rotational levels can be factorized as (Richet et al., 1977)

$$Q = Q_{tr}Q_{vib}Q_{rot}. \quad (10)$$

The translational contribution is identical to that derived for the monoatomic gas (Eq. (5)). The harmonic vibrational contribution is

$$Q_{vib} = \prod_i \frac{e^{-\frac{h\nu_i}{(2kT)}}}{1-e^{-\frac{h\nu_i}{(kT)}}}, \quad (11)$$

where ν_i is a fundamental harmonic vibrational frequency of the isolated molecule. The rotational contribution can be factorized in a classical and in a quantum-mechanical correction term as

$$Q_{rot} = Q_{rot}^{class}Q^{corr}, \quad (12)$$

with

$$Q_{rot}^{class} = \left[\frac{\pi}{\sigma_A\sigma_B\sigma_C}\right]^{1/2}, \quad (13)$$

$$Q^{corr} = 1 + \frac{1}{6}\left(\sigma_A + \sigma_B + \sigma_C - \frac{\sigma_A\sigma_B}{2\sigma_C} - \frac{\sigma_B\sigma_C}{2\sigma_A} - \frac{\sigma_C\sigma_A}{2\sigma_B}\right), \quad (14)$$

$$\sigma_x = \frac{\hbar^2}{2kTI_x}, \quad (15)$$

where I_x is the inertia momentum of the molecule along the x axis (Stripp and Kirkwood, 1951).

Anharmonic corrections to the vibrational term may have important effects in the case of hydrogen (Richet et al., 1977). However, anharmonic calculations are beyond the scope of the present work.

2.2.2. Crystalline solid

In a crystalline solid the phonon frequencies $\nu_{\boldsymbol{q},i}$ are identified by a reciprocal-space vector $\boldsymbol{q}$ and a branch index $i = 1, 3N^{at}$, where N^{at} is the number of atoms in the unit-cell. The harmonic partition function for a unit-cell is

$$Q = \left[\prod_{i=1}^{3N^{at}}\prod_{\{\boldsymbol{q}\}}\frac{e^{-\frac{h\nu_{\boldsymbol{q},i}}{(2kT)}}}{1-e^{-\frac{h\nu_{\boldsymbol{q},i}}{(kT)}}}\right]^{1/N_q}. \quad (16)$$

Here, the second product is performed on a uniform grid of N_q $\boldsymbol{q}$ vectors in the Brillouin zone, for N_q sufficiently large. In the product of Eq. (16), the three $\boldsymbol{q} = \boldsymbol{0}$ translational modes with $\nu_{\boldsymbol{q},i} = 0$ are not considered.

2.3. DFT Calculations

The phonon frequencies used to determine the vibrational free energy are computed using first-principles methods based on density functional theory (DFT) (Hohenberg and Kohn, 1964; Kohn and Sham, 1965). We use the generalized-gradient approximation to the exchange-correlation functional of Perdew, Burke and Ernzerhof (PBE) (Perdew et al., 1996). The ionic cores are described by norm-conserving pseudopotentials (Troullier and Martins, 1991) in the Kleinman–Bylander form (Kleinman and Bylander, 1982). The description of the pseudopotentials is given in the electronic annexes (Table EA-1). In some cases (molecular water and quartz), we performed an additional calculation using the local density approximation (LDA) (Ceperley and Alder, 1980). While, in general, LDA and PBE calculations give similar results, PBE functionals are better suited to model hydrogen-bonded minerals like kaolinite and ice (Lee et al., 1992; Hamann, 1997). For molecular water, quartz and kaolinite, the electronic wave-functions are expanded in plane-waves up to an energy cut-off $\varepsilon_{cut} = 80$ Ry and the charge density cut-off is $4\varepsilon_{cut}$. For ice $\varepsilon_{cut} = 110$ Ry and the charge density cut-off is 1000 Ry. The electronic integration is performed by sampling the Brillouin zone with a $3\times3\times3$ k-point grid for quartz and ice, and with a $2\times2\times2$ k-point grid for kaolinite, according to the Monkhorst–Pack scheme (Monkhorst and Pack, 1976). For molecular water the Brillouin zone sampling is restricted to the Γ-point. In all the cases, atomic positions are obtained after relaxation at zero pressure until the residual forces are less than 10^{-3} Ry/Å. Neither the cell parameters nor the symmetry are constrained during the relaxation.

The vibrational properties are calculated using the linear response theory (Baroni et al., 2001), using the PWSCF package (Baroni et al., http://www.pwscf.org). The phonon frequencies necessary in Eqs. (11) and (16) are obtained following the standard procedure. First, we compute the dynamical matrices exactly (within DFT) on a regular grid of q-vectors. These matrices are then used to determine the interatomic force-constants. Subsequently, the dynamical matrix can be determined in any point of the Brillouin zone by discrete Fourier interpolation of the interatomic force-constants. Long-range effects are taken into account after computing the Born effective-charges and the dielectric constant following Baroni et al. (2001). The treatment is exact for a sufficiently large q-vector grid. The dynamical matrices are computed exactly (within DFT) on a $3\times3\times3$ q-point grid for quartz, on a $2\times2\times2$ grid for kaolinite,

on a $3 \times 3 \times 3$ grid for ice, and only at the Γ-point for water. Then, the vibrational partition function of Eq. (16) is obtained performing the product on a $n \times n \times n$ grid, with $n = 5$ for quartz, $n = 6$ for ice and $n = 7$ for kaolinite.

3. RESULTS AND DISCUSSION

3.1. Relaxed structures

The structure of quartz was relaxed at the LDA and PBE levels. The result shows good agreement with experiment (Will et al., 1988) and consistency with previous computations (Hamann, 1996; electronic annex, Table EA-2). Agreement between the relaxed structure of kaolinite, shown in Table EA-3, and experiment (Bish, 1993) is discussed in Balan et al. (2001). The relaxation of the isolated water molecule was realized in a cubic cell with lattice constant of 16 Å (Table EA-4). The 2% relative elongation of the OH distance with respect to experimental structure (Császár et al., 2005) is typical of PBE calculations (Xu and Goddard, 2004).

Depending on pressure and temperature, ice can assume many different crystal structures. In this work, we focus on the most common form, hexagonal ice Ih, which forms at ambient pressure below 0 °C. Hexagonal ice is, actually, a crystal with static and/or dynamic disorder, i.e., although the atomic configurations differ from one unit-cell to the other, the time- and space-averaged coordinates are highly symmetric. On the average, the oxygen atoms in ice Ih are arranged on a hexagonal lattice, such that each oxygen has four neighboring oxygens in a tetragonal configuration (Lonsdale, 1958). Since the works of Kuhs and Lehman (Kuhs and Lehmann, 1981; Kuhs and Lehmann, 1983; Kuhs and Lehmann, 1987), the mean proton positions are accurately known as well (see Table EA-5).

In our simulations, we are restricted to a static, periodic model of ice which we design to have vibrational properties similar to the disordered phase. As a starting guess, we used model A of Pfrommer et al. (2000): in a cell corresponding to the unit-cell of the oxygen sublattice, we placed four water molecules, the oxygens being placed at their exact symmetric, averaged lattice sites (cf Table EA-5), and the hydrogens being placed at arbitrary sites following the "ice rules" (Pauling, 1935).

The structure is fully relaxed, so that it loses the hexagonal lattice symmetry of the oxygen sublattice: the only symmetry element left is the gliding plane symmetry $(x, y, z) = (y, x, 0.5 + z)$. The result is shown and compared with experimental ice Ih structure in Table EA-5.

In the final relaxed structure the cell parameters and O–O distances are shrunk with respect to their experimental counterparts, as in former calculations on ice (Morrison and Jenkins, 1999; Umemoto et al., 2004). The angles H–O–H are also smaller than experimental values. The reason is probably that the experimentally measured angle is an average over H–O–H and H–O···H angles. This remark is enforced by the comparison with the measurements of Jorgensen et al. (1984) who found an angle D–O–D of 104 in ordered ice VIII. For other quantities the discrepancy is rather small, and of the same order as already observed on other structures.

3.2. Vibrational properties

Agreement between the measured and computed vibrational properties of kaolinite is discussed in Balan et al. (2001). Calculated frequencies of quartz through the whole Brillouin zone (not shown) are in good agreement with previous PBE calculation (Zicovich-Wilson et al., 2004) and underestimate by typically 5% the experimental ones from inelastic neutron scattering (Strauch and Dorner, 1993).

Calculated harmonic frequencies of molecular water (Table 1) present an error of typically 5%. This is consistent with previous PBE calculations (Lindan et al., 1996; Xu and Goddard, 2004). The compensation between the PBE error and the neglect of anharmonicity was already observed in previous computations of hydroxyl frequencies (e.g. Balan et al., 2005). Table 2 presents further analysis of our results: the mode frequencies of different isotopomers of water and the corresponding isotopic shifts, are compared with the experimental values. The relative errors on absolute frequencies and on the difference between the frequency of different isotopomers are of similar magnitude (see Section 3.4).

Concerning ice, following Lee et al. (1993), we calculated the vibrational density of states of ice and identified the contributions of the O–H stretching, H–O–H bending, librational and translational modes (Fig. EA-1) The calculated spectrum is in good agreement with previous DFT calculations (Lee et al., 1993; Morrison and Jenkins, 1999). Measurements from Incoherent Inelastic Neutron Scattering (IINS) (Li, 1996), are compared with our result in Table EA-6.

3.3. β-factors

The results will be discussed in terms of the logarithmic β-factors ($\ln\beta$) and logarithmic fractionation factors ($\ln\alpha$) expressed in parts per thousand (‰), unless stated otherwise. β-factors have been calculated using both Eq. (8) and (6). As Eq. (6) is considered as more precise, only the results from this equation are reported, except when stated. The difference between the results of the two equations is less than 0.1 in all systems except for hydrogen β-factor of ice and gas-water. Logarithmic β-factors have been computed every 0.5 $\frac{10^6}{T^2}$ (in K^{-2}). Those points have been fitted with third order polynoms over different domains of temperature. The domain of interest here is 0–400 °C for the mineral phases and −70 to 0 °C for ice. Fits concerning O and H fractionation for water have been made on 3

Table 1
Water molecule: calculated vs. experimental vibrational frequencies (cm^{-1})

Mode	Experimental		This work	
	Harmonic[a]	Anharmonic[b]	PBE	LDA
Sym. stretch	3835	3657	3640	3679
Asym. stretch	3939	3756	3747	3795
Bond bend	1648	1595	1586	1542

[a] Khachkuruzov (1959).
[b] Lide (1998).

Table 2
Water molecule: calculated vs. experimental harmonic vibrational frequencies (cm^{-1})

Species	$H_2{}^{16}O$	$D_2{}^{16}O$	$H_2{}^{18}O$	$\Delta^{18}O$[a]	ΔD[b]
This work (PBE)					
ω_1	3640	2624	3633	7.62	1016.6
ω_2	3747	2745	3731	15.21	1001.8
ω_3	1586	1161	1580	6.64	424.9
Experimental[c]					
ω_1	3835.37	2762.84	3837.59	7.78	1072.53
ω_2	3938.74	2885.99	3922.69	16.15	1052.75
ω_3	1647.59	1206.72	1640.62	6.97	440.87

[a] $\Delta^{18}O = \omega(H_2{}^{16}O) - \omega(H_2{}^{18}O)$.
[b] $\Delta D = \omega(D_2{}^{16}O) - \omega(H_2{}^{16}O)$.
[c] Khachkuruzov (1959).

different temperature domains, as suggested by Rosenbaum (Rosenbaum, 1997), due to the non-linear behavior of the curve: −70–0 °C , 0–130 °C and 130–400 °C.

The DFPT computed oxygen β-factor of gas water is reported in Fig. 1, where it is compared (in the inset) with harmonic calculation based on the experimental data of Khachkuruzov (1959) and with calculation taking into account anharmonic effects of Richet et al. (1977) (see also Rosenbaum, 1997). The parameters used in the anharmonic calculation of Richet et al. (1977) are the molecular constants obtained by fitting the experimental spectroscopic data of Khachkuruzov (1959). The difference between the harmonic calculation based on the DFPT frequencies and on the experimental harmonic frequencies is 3‰ at 300 K (see inset of Fig. 1). It corresponds to a 4% relative error in lnβ. According to the anharmonic calculations of Richet et al. (1977), the β-factor is 61.1‰ at 300 K, corresponding to a shift of −3‰ related to anharmonicity. This is very close to the harmonic DFPT calculation, the difference being only of 0.8‰. This seemingly good agreement is due to the cancellation of the two errors given by the absence of anharmonic effects in Eq. (10) and the DFPT underestimation of the water-molecule harmonic-frequencies.

β-factors of quartz have been calculated using both LDA and PBE functionals (Fig. 1). The difference between the two calculations provides an insight into the variability of theoretical results that can be obtained with various DFT functionals. The difference between the two is 6‰ at 300 K, corresponding to a 6% relative difference.

The oxygen β-factor in kaolinite has been computed substituting the oxygens belonging to a hydroxyl group (OH), the oxygens not belonging to a hydroxyl group, or both. According to these calculations (Fig. 1), the properties of the two different sites are significantly different, due to the different chemical properties, and bonding strength.

The hydrogen β-factors have been calculated for gas water, ice and kaolinite (Fig. 2). The difference between calculations using Eqs. (8) and (6) is dramatic in the case of molecular water and ice. For those, the difference between the two formulas reaches respectively 25‰ and 11‰ at 300 K. It is well established that, for gas water, Eq. (6) is correct in the case of a dilute deuterium content (Richet

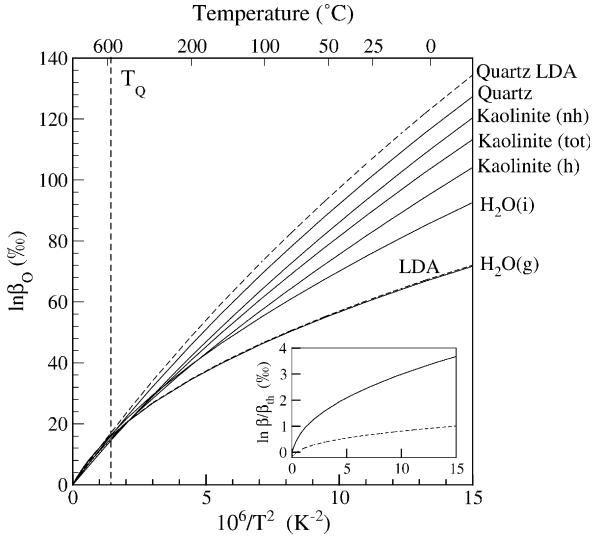

Fig. 1. Oxygen β-factors obtained from Eq. (6). Calculations are done using PBE (continuous lines) or LDA (dashed lines). H_2O(i): ice-water. H_2O(g): gas-water (isolated molecule). Kaolinite (h): oxygens belonging to a hydroxyl group in kaolinite. Kaolinite (nh): oxygens not belonging to a hydroxyl group in kaolinite. Kaolinite (tot): total oxygen β-factor in kaolinite. T_Q is the stability limit temperature for α-quartz structure. It corresponds also approximately to the limit of stability of kaolinite. Insert: logarithmic difference between our theoretical β-factor of gas water (β_{th}) and previous β-factors derived using experimental molecular constants and harmonic (continuous line: data from Khachkuruzov, 1959) or anharmonic (dashed line: Richet et al., 1977) calculations.

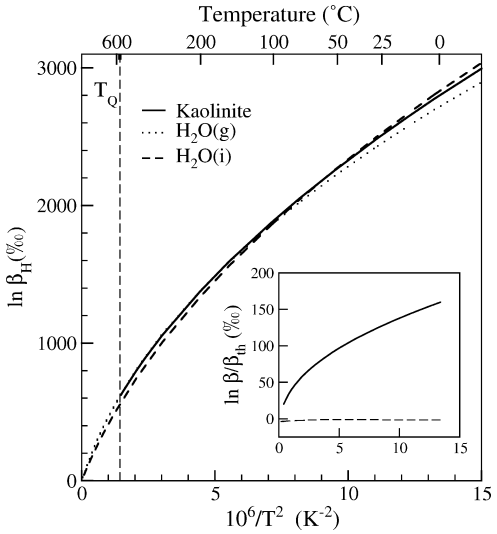

Fig. 2. Hydrogen β-factors obtained from Eq. (6), for kaolinite, gas and ice water. T_Q corresponds to the limit of stability of kaolinite. Insert: logarithmic difference between our theoretical β-factor of gas water (β_{th}) and previous β-factors derived using experimental molecular constants and harmonic (continuous line: data from Khachkuruzov, 1959) or anharmonic (dashed line: Richet et al., 1977) calculations.

et al., 1977). For ice, this is also true because this material is made essentially of H-bonded water molecules. In the case of kaolinite, the difference between the results of the two equations is 0.2‰. This small difference corresponds to a 10^{-4} relative error in $\ln\beta$, similar to what is observed for oxygen β-factors. Nevertheless, the fact that the β-factors of hydrogen are very large makes this difference not negligible with respect to measurements.

Hydrogen β-factor of molecular water shown in Fig. 2 has been calculated with frequencies from Table 2. The result is compared with harmonic and anharmonic calculations based on the experimental molecular constants of water (see inset of Fig. 2). The difference between anharmonic curve from Richet et al. (1977) and this work is very small: around 1‰ at 300 K. The difference between β-factors calculated using experimental and calculated harmonic frequencies is large and reaches 150‰ at 300 K (see inset of Fig. 2).

β-factors related to silicon (not shown here) have been calculated in the same way. They vary monotonically between 0 and typically 80‰ at 273 K, for quartz and kaolinite.

3.4. Uncertainty in theoretical β-factors

Numerical errors due to the choice of the cut-off energy and k-point sampling for the phonon energy calculations are well documented in literature for the systems under consideration. We checked that their influence is negligible for the results shown in the present study. As an example, in Table EA-7 of the electronic annexes we report the computed values of the oxygen β-factor for quartz as a function of these parameters. As a further example, in Table 3 we report the dependence of oxygen β-factor for quartz as a function of the grid used for the dynamical-matrix calculation and to perform the product in Eq. (16). Again, the numerical error due to the choice of these parameters is negligible.

The accuracy of the calculated β-factor values depends primarily on two factors: error of the DFPT on the calculated phonon frequencies between isotopomers, and anharmonic effects. The performance of the generalized gradient approximation (PBE functionals, used here) on phonon calculations, has been tested by Favot and Dal Corso (1999) and Dal Corso and de Gironcoli (2000). It was found that the frequencies calculated are in agreement with experiment on a large variety of systems. On average, the PBE calculations reproduce the frequencies with a systematic underestimation depending on the system, from 2 to 5 relative % (Favot and Dal Corso, 1999; Schauble et al., 2006). To correct those systematic deviations, two approaches have been proposed.

First, multiplying the frequencies by a scaling factor in order to match the experimentally measured frequencies. This approach is meaningful for closely related minerals (Schauble et al., 2006 for carbonates; Zeebe, 2005 for borates), which present comparable deviations, and when accurate spectroscopic data are available. It is thus not fully predictive. In addition, the use of a scaling factor has only a very small effect on the final result, i.e. the equilibrium isotopic fractionation constants, due to cancellation of systematic errors (Schauble et al., 2006).

Another approach is based on the assumption that the PBE underestimation of phonon frequencies is related to an overestimation of lattice constants (Favot and Dal Corso, 1999). It is thus possible to perform phonon calculation using the experimental structure, or to rescale the relaxed structure to experimental cell parameters (Balan et al., 2001, 2002, 2005). This approach improves the comparison of theoretical calculation with experimental IR or Raman spectrum, but can produce structural instabilities, biasing some of the vibrational branches. To avoid such a problem, fully relaxed structures are used. Therefore, error on phonon frequencies introduced by the DFT calculation, at the LDA or PBE levels, can be essentially described as a systematic relative error of about 5%. This error is similar to that affecting the calculation of β-factors (Table 2). The contribution of anharmonicity in the β-factor can be discussed with reference to data on the water molecule. The anharmonic contribution is equal to −3‰ for oxygen β-factor and −150‰ for hydrogen β-factor, both corresponding to −5% relative effect. However, water molecule is strongly anharmonic and anharmonic effects are expected to be smaller for other systems. To summarize, the error on isotopic fractionation factors induced by DFT or anharmonicity should not exceed some relative percents, thanks to the cancellation of systematic errors between the frequencies derived for isotopomers.

Table 3
Logarithm of the oxygen β-factor of the SiO_2 quartz (‰) at $T = 300$ K

	$m = 1$	$m = 3$
$n = 2$	100.312	100.418
$n = 3$	100.311	100.419
$n = 4$	100.310	100.418
$n = 7$	100.309	100.417

Calculations are done using the PBE functional. The dynamical matrix are first computed exactly (within DFT) on a $m \times m \times m$ grid. Then, the vibrational partition function of Eq. (16), are obtained performing the product on a $n \times n \times n$ grid (see Section 2.3).

3.5. Isotopic fractionation

Logarithmic fractionation laws deduced from the fits of the β-factors are reported in Table 4.

3.5.1. Oxygen fractionation

3.5.1.1. Ice/gas-water. The theoretical oxygen fractionation factor between ice and gas water (Fig. 3) is compared to the experimental measurements by Majoube (1970). The calculation accurately reproduces the slope of the experimental law, and the difference between theoretical calculation and experimental data is small (+3.3‰ at 273 K).

3.5.1.2. Quartz/liquid-water. Direct calculation of liquid water thermodynamical properties is computationally very demanding. The theoretical and experimental fractionation

Table 4
Fits of 1000 lnα based on the function $a + bx + cx^2 + dx^3$, with $x = 10^6/T^2$

Element	Phases	T (°C)	a	b	c	d
$^{18}O/^{16}O$	Quartz–H_2O(g)	0–130	−9.6341	4.848	−0.0382	0.000397
	Quartz–H_2O(g)	130–400	−2.9548	1.342	0.6062	−0.040638
	Kaolinite (tot)–H_2O(g)	0–130	−8.5918	3.276	0.0089	−0.000236
	Kaolinite (tot)–H_2O(g)	130–400	−1.9125	−0.230	0.6533	−0.041271
	H_2O(i)–H_2O(g)	−70–0	−2.685	1.675	− 0.00721	−0.0016799
	Kaolinite (nh)–Kaolinite (h)	0–400	−2.810	1.192	0.0343	− 0.001998
D/H	Kaolinite–H_2O(g)	0–130	−21.18	0.97	0.7512	− 0.01925
	Kaolinite–H_2O(g)	130-400	14.76	−24.02	6.684	− 0.49189
	H_2O(i)–H_2O(g)	−70–0	−144.37	20.74	− 0.1203	0.000193
$^{30}Si/^{28}Si$	Quartz–Kaolinite	0–400	0.0230	0.1796	−0.0045	0.000099

See caption of Fig. 1.

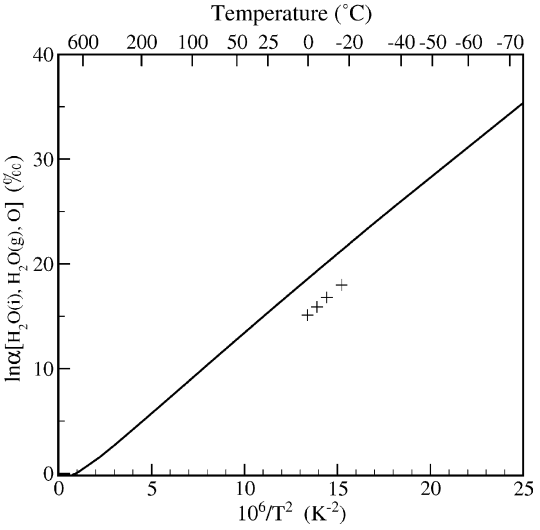

Fig. 3. Theoretical oxygen isotope fractionation factor between ice and gas water (solid line). Crosses: experimental data from Majoube, 1970.

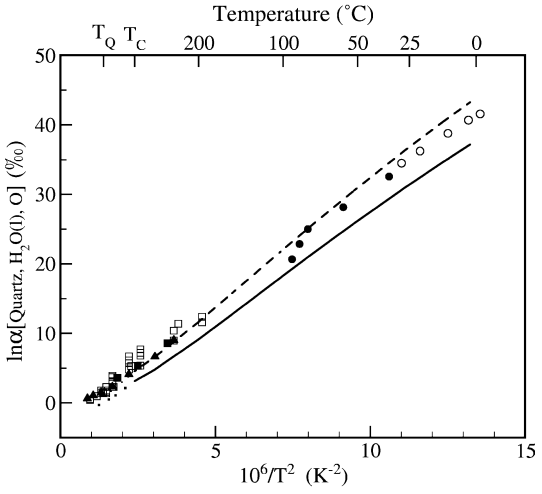

Fig. 4. Theoretical oxygen isotopic fractionation factor between quartz and liquid water, H_2O(l). Solid line: PBE calculation. Dashed line: LDA calculation. Symbols correspond to experimental data (open circles: Labeyrie, 1974; solid circles: Kita et al., 1985; open squares: Clayton, 1972; solid squares: Matthews and Beckinsale, 1979, solid triangles: Matsuhisa et al., 1979). T_C is the critical temperature of liquid water. Below T_C we represent the fractionation between quartz and gas water (dotted line). T_Q is the stability limit of α-quartz at ambient pressure.

factors derived between ice- and gas-water are, however, in good agreement. Therefore, we decided to use a hybrid approach and the fractionation quartz/liquid-water (Fig. 4) is calculated from the theoretical quartz/gas-water fractionation and the experimental liquid/gas-water fractionation, determined by Horita and Wesolowski (1994). Note that the contribution of liquid/gas-water fractionation is smaller than that of ice/gas-water. For example, at 300 K, the two contributions are, respectively, 9.2 and 40.1, giving a resulting mineral–liquid water fractionation of 30.9. The root mean square error reported by Horita and Wesolowski (1994) for the experimental law is 0.11‰, which is much smaller than theoretical uncertainties. The PBE calculation of the quartz/liquid-water fractionation is in very good agreement with the experimental curve over the whole domain of temperature. The difference between the two is 3.5‰ at 300 K, consistent with the uncertainty of theoretical frequencies. In Fig. 4, LDA calculations are also reported. At low temperatures, LDA and PBE calculations are flanking the experimental result. Difference between the two calculations is 5.5‰ at 300 K.

3.5.1.3. Kaolinite/liquid-water. The isotopic fractionation in two well-constrained systems, ice/gas-water and quartz/liquid-water are correctly reproduced by DFT calculations. This suggests that isotopic fractionation factors of oxygen can be reproduced within an accuracy of typically 3–4‰. As expected, the theoretical fractionation between kaolinite and water (Fig. 5) is close to the measurements at high temperature. For this system, the dispersion of the measurements is however larger. At 20 °C, the difference between calculation and measurements (Savin and Epstein, 1970; Lawrence and Taylor, 1972) becomes significant (about 5‰). This suggests that low temperature measurements could overestimate the equilibrium fractionation factor.

3.5.1.4. Kaolinite internal fractionation. For kaolinite, we computed the internal-fractionation of oxygen isotopes

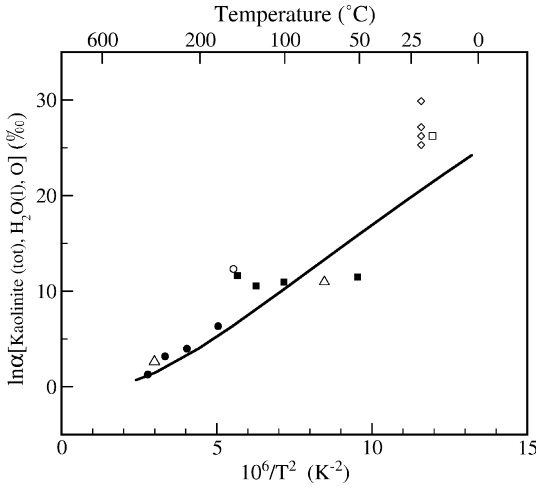

Fig. 5. Theoretical oxygen isotopic fractionation factor between kaolinite and liquid water (solid line). Symbols correspond to experimental data (open circles: Eslinger et al., 1971; solid circles: Kulla and Anderson, 1978; open squares: Lawrence and Taylor, 1972; solid squares: Marumo et al., 1982; diamonds: Savin and Epstein, 1970; triangles: Sheppard et al., 1969).

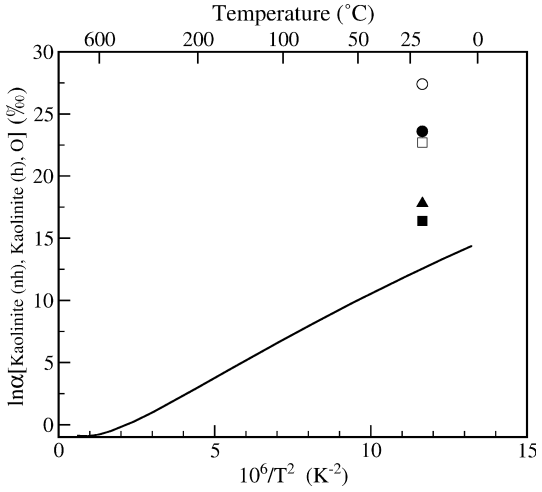

Fig. 6. Theoretical non-hydroxyl/hydroxyl oxygen intracrystalline kaolinite fractionation factor (solid line). Symbols correspond to fractionation factors calculated from experimental data (open circles: Girard and Savin, 1996; solid circles: Bechtel and Hoernes, 1990; open squares: Hamza and Epstein, 1980; solid squares: Hamza and Epstein, 1980 using non-OH isotopic composition (see text); solid triangles: Savin, 1967).

between sites belonging to a hydroxyl group and sites not belonging to a hydroxyl group (Fig. 6). As suggested by Girard and Savin (1996), the internal-fractionation of oxygen between hydroxyl and non-hydroxyl sites in kaolinite can be a useful in situ geothermometer.

We remark that the calculation of the fractionation between different sites in the same material is more consistent than the one implying two different systems. In fact, possible systematic errors due the choice of the functional are canceled out. As a consequence, we expect calculations of Fig. 6 to be more precise than calculations involving two different minerals. Accordingly, experimental data (Savin, 1967; Hamza and Epstein, 1980; Bechtel and Hoernes, 1990; Girard and Savin, 1996) are probably overestimations of the internal fractionation of ^{18}O.

This observation could bring new insight for the interpretation of experimental data. Experimental data are obtained from the measurement of the isotopic composition $\delta^{18}O_{bulk}$ and one of the two other quantities $\delta^{18}O_{OH}$ and $\delta^{18}O_{non\text{-}OH}$ (for a definition see, e.g., Girard and Savin, 1996). The different fractionation-factors deduced from available measurements are summarized in Table 5. The best agreement with the present calculations is found using $\delta^{18}O_{bulk}$ and $\delta^{18}O_{non\text{-}OH}$ measured by Hamza and Epstein (1980). As the accuracy of $\delta^{18}O_{bulk}$ is *a priori* very good, the present findings suggest that the different measurements (done with both partial fluorination or thermal dehydroxylation) of $\delta^{18}O_{OH}$ are systematically underestimated. The probable origin of this underestimation is the presence of kinetic effects. Concluding, the present calculations suggest that a high-temperature fluorination of the remaining material successive to a low-temperature fluorination, intended to extract hydroxyl oxygens, could give a fairly accurate value of $\delta^{18}O_{non\text{-}OH}$. We remark that the value of $\delta^{18}O_{non\text{-}OH}$ reported by Hamza and Epstein (1980) is the only one of this type reported in literature.

3.5.2. Hydrogen fractionation

3.5.2.1. Ice/gas-water. The computed hydrogen fractionation between ice and gas-water precisely reproduces the experimental data (Fig. 7).

The difference between the slope of the theoretical and measured curves is negligible, whereas the difference between measurements and theoretical curve is typically of 8–10‰, corresponding to a 6% relative error. The dispersion of experimental data is typically 2‰. In this case, the accuracy of the DFT calculation is significantly better than what is suggested by uncertainties on the β-factor (150‰ variation for the hydrogen β-factor of gas water). For this system, the assumption that the relative error on frequencies propagate on the final result is verified. Moreover, anharmonic effects do not have a critical importance, being the anharmonicity in the bonds of ice and gas-water similar.

3.5.2.2. Kaolinite/liquid-water. The hydrogen fractionation between kaolinite and liquid-water (Fig. 8) is determined from the computed kaolinite/gas-water fractionation and the experimental liquid/gas-water fractionation determined by Horita and Wesolowski (1994). The relative contribution of liquid/gas-water fractionation is greater for hydrogen than for oxygen. For example, at 300 K, the computed kaolinite/gas-water fractionation is 56.26‰, whereas the liquid/gas-water fractionation is equal to 73.97‰ (from the experimental fit given by Horita and Wesolowski (1994)) leading to a kaolinite/liquid-water fractionation of −17.71‰. Therefore, the experimental uncertainties could significantly contribute to the final error. In fact, the deviation between the regression law proposed by Horita and Wesolowski (1994), and the experimental

Table 5
Experimental internal-fractionation of oxygen in kaolinite

Source	Method[a]	$\delta^{18}O_{bulk}$	$\delta^{18}O_{OH}$	$\delta^{18}O_{non\text{-}OH}$	1000 ln α[Kaolinite (nh), Kaolinite (h), O] (a)	(b)	(c)	
Savin (1967)	PF	21.0	11.1		17.8			
Hamza and Epstein (1980)	PF	21.2	8.6	28.5	22.7	16.4	19.9	
Bechtel and Hoernes (1990)	PF, TD	18.4	5.3		23.6			
Girard and Savin (1996)	TD	21.7	6.5		27			
Theory								12.5

(a) Calculated from $\delta^{18}O_{bulk}$ and $\delta^{18}O_{OH}$.
(b) Calculated from $\delta^{18}O_{bulk}$ and $\delta^{18}O_{non\text{-}OH}$.
(c) Calculated from $\delta^{18}O_{OH}$ and $\delta^{18}O_{non\text{-}OH}$.
[a] Analytical technique: PF, partial fluorination; TD, thermal dehydroxylation.

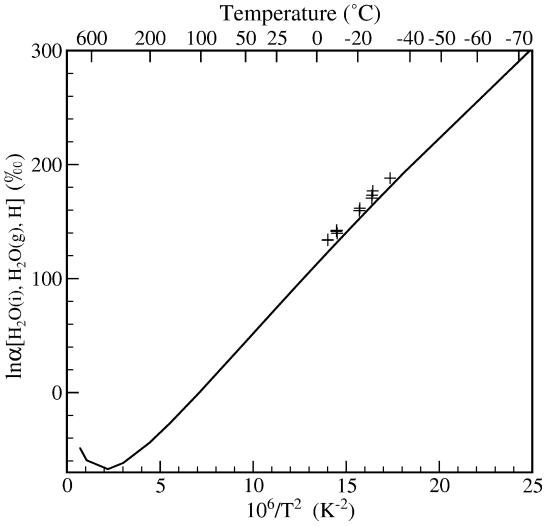

Fig. 7. Theoretical hydrogen isotope fractionation factor between ice and gas water (solid line). Crosses: experimental data from Merlivat and Nief (1967).

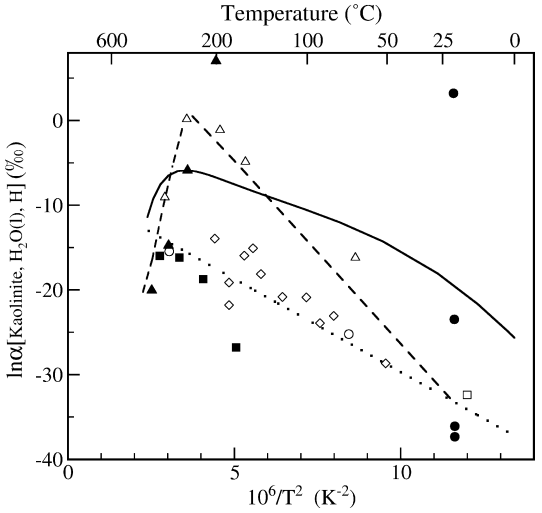

Fig. 8. Theoretical hydrogen isotopic fractionation factor between kaolinite and liquid water (solid line). Symbols correspond to experimental data (open circles: Sheppard et al., 1969; solid circles: Savin and Epstein, 1970; open squares: Lawrence and Taylor, 1972; diamonds: Marumo et al., 1980; open triangles: Lambert and Epstein, 1980; solid triangles: Liu and Epstein, 1984). Proposed experimental fits [dashed line: Lambert and Epstein, 1980; dotted line: Gilg and Sheppard, 1996] are shown for comparison.

measurements reaches ±4‰ (Horita and Wesolowski, 1994), with $\sigma = 1.2$‰.

The measurements of the kaolinite/liquid-water fractionation show significant scattering. Nevertheless, a comparison can be done between the DFT calculation and the two proposed experimental fits (Fig. 8). The low-temperature part of the DFT curve is consistent with the monotonic behavior and the slope proposed by Gilg and Sheppard (1996), with a shift of +13–14‰. In contrast, the shape of the curve is far from monotonic at high temperature, accrediting the hypothesis of a more complex curve as proposed by Lambert and Epstein (1980). The maximum of the curve occurs between 250 and 270 °C, to be compared with 230 °C as proposed by Lambert and Epstein (1980).

3.5.3. Silicon fractionation: kaolinite/quartz

Theoretical calculations (Fig. 9) attest of a significant equilibrium fractionation of silicon isotopes between kaolinite and quartz, which reaches 1.6‰ at 300 K. Following the observations made above on oxygen and hydrogen, we expect the relative error on the theoretical fractionation-factors to be smaller than 10%. To our knowledge, no measurements of the isotopic fractionation of silicon between kaolinite and quartz are available. However, the regularities of silicon-isotope variations have been studied recently (e.g. Ding et al., 1996), which reports a fractionation of 0.2–0.4‰ between quartz and biotite in granitic rocks.

The DFT calculation is in agreement with the two general tendencies stated for silicon fractionation: (i) the silicon-rich phase is enriched in ^{30}Si with respect to the silicon-poor phase; (ii) the ^{30}Si content increases with the degree of silicate polymerization. Those tendencies are suggested both by experimental observations (Douthitt, 1982; Ding et al., 1996), theoretical calculations on minerals (Grant, 1954), and general considerations on vibrational properties of silicates (Ding et al., 1996, p. 60). However, the calculation of Grant (1954), which correctly pointed out the variation trends of Si fractionation, likely provided overestimated values of fractionation factors. Theoretical equilibrium isotopic fractionation factors of Si, combined with measurements on reference systems, should bring important constraints to interpret the budget of Si isotopes

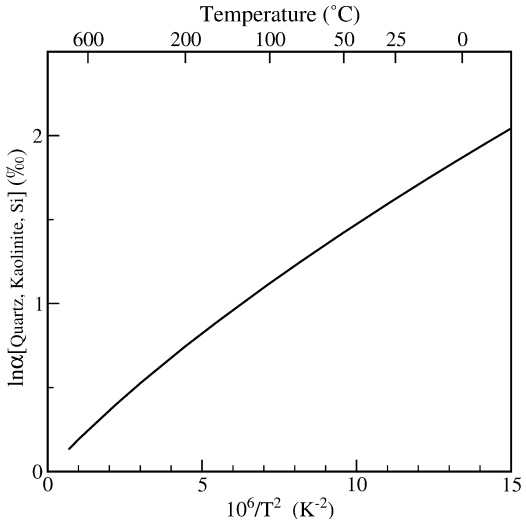

Fig. 9. Theoretical quartz–kaolinite silicon fractionation curve.

during the evolution of Earth crust and Si transfers from the crust to other pools, such as mantle rocks, oceanic waters or biosphere.

4. CONCLUSIONS

We have exposed a general method to compute solid-state isotopic fractionation using first-principles calculations. This method has been validated on well-constrained model systems, for which it provides isotopic fractionation factors in very good agreement with available experimental values. For the considered systems, a wide set of measurements of vibrational properties is available. This could be used to construct models to obtain an even better estimation of the isotopic fractionation. However, we remark that the goal of the present paper is the validation of a fully first-principles approach which could be applied to further systems that are not characterized experimentally so well. The present approach allows the study of issues with major importance in geochemistry, such as silicon equilibrium fractionation, and to assess the consistency between observed fractionation and thermodynamical equilibrium conditions.

ACKNOWLEDGMENTS

We thank E. Schauble and an anonymous reviewer for their constructive comments which improved the paper. Fruitful discussions with P. Agrinier (Université Paris VII), F. Guyot (Université Paris VII) and F. Poitrasson (LMTG-Toulouse) are gratefully acknowledged. This work was supported by the French ANR project SPIRSE and Eurocores Eurominsci project HYDROMIN. This is IPGP contribution n°2218. Calculations were performed at IDRIS (Orsay, France), within the project n°060411519.

APPENDIX A. SUPPLEMENTARY DATA

Supplementary data associated with this article can be found, in the online version, at doi:10.1016/j.gca.2007.04.012.

REFERENCES

Alexandre A., Meunier J. D., Llorens E., Hill S. M., and Savin S. M. (2004) Methodological improvements for investigating silcrete formation: petrography, FT-IR and oxygen isotope ratio of silcrete quartz cement, Lake Eyre Nasin (Australia). *Chem. Geol.* **211**, 261–274.

Balan E., Lazzeri M., Morin G., and Mauri F. (2006) First-principles study of the OH-stretching modes of gibbsite. *Am. Mineral.* **91**, 115–119.

Balan E., Lazzeri M., Saitta A. M., Allard T., Fuchs Y., and Mauri F. (2005) First-principles study of OH-stretching modes in kaolinite, dickite, and nacrite. *Am. Mineral.* **90**, 50–60.

Balan E., Saitta A. M., Mauri F., and Calas G. (2001) First-principles modeling of the infrared spectrum of kaolinite. *Am. Mineral.* **86**, 1321–1330.

Balan E., Saitta A. M., Mauri F., Lemaire C., and Guyot F. (2002) First-principles calculation of the infrared spectrum of lizardite. *Am. Mineral.* **87**, 1286–1290.

Baroni S., de Gironcoli S., and Corso A. D. (2001) Phonons and related crystal properties from density-functional theory. *Rev. Mod. Phys.* **73**, 515–562.

Bechtel A., and Hoernes S. (1990) Oxygen isotope fractionation between oxygen of different sites in illite minerals: a potential single-mineral thermometer. *Contrib. Mineral. Petrol.* **104**, 463–470.

Bish D. L. (1993) Rietveldt refinement of the kaolinite structure at 1.5 K. *Clays Clay Miner.* **41**, 738–744.

Ceperley D., and Alder B. (1980) Ground state of the electron gas by a stochastic method. *Phys. Rev. Lett.* **45**, 566–569.

Chacko T., Cole D. R., and Horita J. (2001) Equilibrium oxygen, hydrogen and carbon isotope fractionation factors applicable to geologic systems. In *Reviews in Mineralogy and Geochemistry 43: Stable Isotope Geochemistry*, vol. 43 (ed. J. W. Valley), pp. 1–81. Mineral. Soc. America.

Clayton R. N. (1972) Oxygen isotope exchange between quartz and water. *J. Geophys. Res.* **77**, 3057.

Császár A. G., Czakó G., Furtenbacher T., Tennyson J., Szalay V., Shirin S. V., Zobov N. F., and Polyansky O. G. (2005) On equilibrium structures of the water molecule. *J. Chem. Phys.* **122**, 214305.

Dal Corso A., and de Gironcoli S. (2000) Ab initio phonon dispersions of Fe and Ni. *Phys. Rev. B* **62**, 273–277.

Ding T., Jiang S., Wang D., Li J., Song H., Liu Z., and Lao X. (1996) *Silicon Isotope Geochemistry*. Geological Publishing House.

Douthitt C. B. (1982) The geochemistry of the stable isotopes of silicon. *Geochim. Cosmochim. Acta* **46**, 1449–1458.

Dove M. T., Winkler B., Leslie M., Harris M. J., and Salje E. K. H. (1992) A new interatomic potential model for calcite: applications to lattice dynamics studies, phase transition, and isotope fractionation. *Am. Mineral.* **77**, 244–250.

Eslinger, E. V. (1971) Mineralogy and oxygen isotope ratios of hydrothermal and low-grade metamorphic argillaceous rocks. Ph.D. thesis, Case Western Reserve University, USA.

Favot F., and Dal Corso A. (1999) Phonon dispersion: performance of the generalized gradient approximation. *Phys. Rev. B* **60**, 11427.

Gilg H. A., and Sheppard S. M. F. (1996) Hydrogen isotope fractionation between kaolinite and water revisited. *Geochim. Cosmochim. Acta* **60**, 529–533.

Girard J. P., Freyssinet P., and Chazot G. (2000) Unraveling climatic changes from intraprofile variation in oxygen and hydrogen isotopic composition of goethite and kaolinite in laterites: an integrated study from Yaou, French Guiana. *Geochim. Cosmochim. Acta* **64**, 400–426.

Girard J. P., and Savin S. M. (1996) Intracrystalline fractionation of oxygen isotopes between hydroxyl and non-hydroxyl sites in kaolinite measured by thermal dehydroxylation and partial fluorination. *Geochim. Cosmochim. Acta* **60**, 469–487.

Gonze X., Charlier J. C., Allan D. C., and Teter M. P. (1994) Interatomic force constants from first-principles: the case of α-quartz. *Phys. Rev. B* **50**, 13035–13038.

Grant F. (1954) The geological significance of variations in the abundances of the isotopes of silicon in rocks. *Geochim. Cosmochim. Acta* **5**, 225–242.

Hamann D. R. (1996) Generalized gradient theory for silica phase transitions. *Phys. Rev. Lett.* **76**, 660.

Hamann D. R. (1997) H_2O hydrogen bonding in density-functional theory. *Phys. Rev. B* **55**, 10157.

Hamza M. S., and Epstein S. (1980) Oxygen isotopic fractionation between oxygen of different sites in hydroxyl-bearing silicate minerals. *Geochim. Cosmochim. Acta* **44**, 173–182.

Hohenberg P., and Kohn W. (1964) Inhomogeneous electron gas. *Phys. Rev.* **136**, 864–871.

Horita J., and Wesolowski D. J. (1994) Liquid–vapor fractionation of oxygen and hydrogen isotopes of water from the freezing to the critical temperature. *Geochim. Cosmochim. Acta* **58**, 3425–3437.

James A., and Baker D. (1976) Oxygen isotope exchange between illite and water at 22 °C. *Geochim. Cosmochim. Acta* **40**, 235–239.

Jorgensen J. D., Beyerlein R. A., Watanabe N., and Worlton T. G. (1984) Structure of D_2O ice VIII from in situ powder neutron diffraction. *J. Chem. Phys.* **81**, 3211.

Kawabe I. (1978) Calculation of oxygen isotope fractionation in quartz–water system with special reference to the low temperature fractionation. *Geochim. Cosmochim. Acta* **42**, 613–621.

Khachkuruzov G. A. (1959). *Gos. Inst. Prikl. Khim.* **42**, 51–131.

Kieffer S. W. (1982) Thermodynamics and lattice vibrations of minerals. 5. Applications to phase equilibria, isotopic fractionation, and high-pressure thermodynamic properties. *Rev. Geophys. Space Phys.* **20**, 827–849.

Kita I., Taguchi S., and Matsubaya O. (1985) Oxygen isotope fractionation between amorphous silica and water at 34–93 °C. *Nature* **314**, 83–84.

Kleinman L., and Bylander D. M. (1982) Efficacious form for model pseudopotentials. *Phys. Rev. Lett.* **48**, 1425–1428.

Kohn W., and Sham L. (1965) Self-consistent equations including exchange and correlation effects. *Phys. Rev.* **140**, 1133–1138.

Kuhs W. F., and Lehmann M. S. (1981) Bond length, bond angle and transition barrier in ice Ih by neutron scattering. *Nature* **294**, 432–434.

Kuhs W. F., and Lehmann M. S. (1983) The structure of ice Ih by neutron diffraction. *J. Phys. Chem.* **87**, 4312–4313.

Kuhs W. F., and Lehmann M. S. (1987) The geometry and orientation of the water molecule in ice Ih. *J. Phys.* **48**, 3–8.

Kulla J. B., and Anderson T. F. (1978). *Experimental oxygen isotope fractionation between kaolinite and water*, 234.

Labeyrie L. J. (1974) New approach to surface seawater paleotemperatures using $^{18}O/^{16}O$ ratios in silica of diatom frustules. *Nature* **248**, 40–42.

Lambert S. J., and Epstein S. (1980) Stable isotope investigations of an active geothermal system in valles caldera, Jemez Mountains, New Mexico. *J. Volcan. geotherm. Res.* **8**, 111–129.

Lawrence J. R., and Taylor H. P. J. (1972) Hydrogen and oxygen isotope systematics in weathering profiles. *Geochim. Cosmochim. Acta* **36**, 1377–1393.

Lee C., Vanderbilt D., Laasonen K., Car R., and Parinello M. (1992) Ab initio studies on high-pressure phases of ice. *Phys. Rev. Lett.* **69**, 462–465.

Lee C., Vanderbilt D., Laasonen K., Car R., and Parinello M. (1993) Ab initio studies on the structural and dynamical properties of ice. *Phys. Rev. B* **47**, 4863.

Li J. (1996) Inelastic neutron scattering studies of hydrogen bonding in ices. *J. Chem. Phys.* **105**, 6733.

Lide, D.R. (ed.) (1998) *CRC Handbook*, 79th ed. CRC Press, London, pp. 9–76.

Lindan P. J. D., Harrison N. M., Holender J. M., and Gillan M. J. (1996) First-principles molecular dynamics simulation of water dissociation on TiO_2. *Chem. Phys. Lett.* **261**, 246–252.

Liu K. K., and Epstein S. (1984) The hydrogen isotope fractionation between kaolinite and water. *Chem. Geol.* **2**, 335–350.

Lonsdale D. K. (1958) The structure of ice. *Proc. R. Soc. London, Ser. A* **247**, 424–434.

Majoube M. (1970) Fractionation factor of ^{18}O between water vapor and ice. *Nature* **226**, 1242.

Marumo K., Matsuhisa Y., and Nagasawa K. (1982) Hydrogen and oxygen isotopic compositions of kaolin minerals in Japan. *Dev. Sedimentol.* **35**, 315–320.

Marumo K., Nagasawa K., and Kuroda Y. (1980) Mineralogy and hydrogen isotope geochemistry of clay minerals in the Ohnuma geothermal area, northeastern Japan. *Earth. Planet. Sci. Lett.* **47**, 255–262.

Matsuhisa Y., Goldsmith J. R., and Clayton R. N. (1978) Mechanisms of hydrothermal crystallization of quartz at 250 °C and 15 kbars. *Geochim. Cosmochim. Acta* **42**, 173–182.

Matsuhisa Y., Goldsmith J. R., and Clayton R. N. (1979) Oxygen isotopic fractionation in the system quartz–albite–anorthite–water. *Geochim. Cosmochim. Acta* **43**, 1131–1140.

Matthews A., and Beckinsale R. D. (1979) Oxygen isotope equilibration systematics between quartz and water. *Am. Mineral.* **64**, 232–240.

Merlivat L., and Nief G. (1967) Fractionnement isotopique lors des changements d'état solide-vapeur et liquide-vapeur de l'eau à des températures inférieures à 0 °C. *Tellus* **19**, 122.

Monkhorst H. J., and Pack J. D. (1976) Special points for Brillouin-zone integrations. *Phys. Rev. B* **13**, 5188–5192.

Morrison I., and Jenkins S. (1999) First principles lattice dynamics studies of the vibrational spectra of ice. *Physica B*, 442–444.

Nordt L. C., Kelly E. F., and Chadwick O. A. (1998) Biogeochemistry of isotopes in soil environments: theory and application. *Geoderma* **82**, 1–3.

O'Neil J. R., and Kharaka Y. K. (1976) Hydrogen and oxygen isotope exchange reactions between clay minerals and water. *Geochim. Cosmochim. Acta* **40**, 241–246.

Patel A., geoffrey D. Pric, and Mendelssohn M. J. (1991) A computer simulation approach to modelling the structure, thermodynamics and oxygen isotope equilibria of silicates. *Phys. Chem. Minerals* **17**, 690–699.

Pauling L. (1935) The structure and entropy of ice and of other crystals with some randomness of atomic arrangement. *J. Amer. Chem. Soc.* **57**, 2680–2684.

Perdew J. P., Burke K., and Ernzerhof M. (1996) Generalized gradient approximation made simple. *Phys. Rev. Lett.* **77**, 3685–3868.

Pfrommer B. G., Mauri F., and Louie S. G. (2000) NMR chemical shifts of ice and liquid water: the effects of condensation. *J. Amer. Chem. Soc.* **122**, 123–129.

Richet P., Bottinga Y., and Javoy M. (1977) A review of hydrogen, carbon, nitrogen, oxygen, and chlorine stable isotope fractionation among gaseous molecules. *Ann. Rev. Earth Planet. Sci.* **5**, 65–110.

Rignanese G. M., and Gonze X. (2001) First-principles study of structural, electronic, dynamical, and dielectric properties of zircon. *Phys. Rev. B* **63**, 104305.

Rosenbaum J. M. (1997) Gaseous, liquid and supercritical fluid H_2O and CO_2: oxygen isotope fractionation behavior. *Geochim. Cosmochim. Acta* **61**, 4993–5003.

Rosenthal J. E. (1935) Vibrations of symmetrical tetratomic molecules. *Phys. Rev.* **47**, 235–237.

Savin, S. M. (1967) Oxygen and hydrogen isotope ratio in sedimentary rocks and minerals. Ph.D. thesis, Californian Institute of technology.

Savin S. M., and Epstein S. (1970) The oxygen and hydrogen isotope geochemistry of clay minerals. *Geochim. Cosmochim. Acta* **34**, 25–42.

Schauble E. A., Ghosh P., and Eiler J. M. (2006) Preferential formation of ^{13}C-^{18}O bonds in carbonate minerals, estimated using first-principles lattice dynamics. *Geochim. Cosmochim. Acta* **70**, 2510–2529.

Shaffer W. H., and Schuman R. P. (1944) The infra-red spectra of Bent XYZ molecules part I. Vibration–rotation energies. *J. Chem. Phys.* **12**, 504–513.

Sheppard S. M. F., and Gilg H. A. (1996) Stable isotope geochemistry of clay minerals. *Clay Miner.* **31**, 1–24.

Sheppard S. M. F., Nielsen R. L., and Taylor H. P. J. (1969) Oxygen and hydrogen isotope ratios of clay minerals from porphyry copper deposits. *Econ. Geol.* **64**, 755–777.

Strauch D., and Dorner B. (1993) Lattice dynamics of α-quartz: I. Experiment. *J. Phys.: Condens. Matter* **5**, 6149–6154.

Stripp K. F., and Kirkwood J. G. (1951) Asymptotic expansion of the partition function of the asymmetric top. *J. Chem. Phys.* **19**, 1131–1133.

Troullier N., and Martins J. (1991) Efficient pseudopotentials for plane-wave calculations. *Phys. Rev. B* **43**, 1993–2006.

Umemoto K., Wentzcovitch R. M., Baroni S., and de Gironcoli S. (2004) Anomalous pressure-induced transitions in ice XI. *Phys. Rev. Lett.* **92**, 105502.

Urey H. C. (1947) The thermodynamic properties of isotopic substances. *J. Chem. Soc. (Lond.)*, 562–581.

Valley, J.W., Taylor, H.P.J. and O'Neil, J.R. (eds.) (1986). *Stable isotopes in high temperature geological processes Rev Mineral*, vol.16. Mineralogical society of america.

Will G., Bellotto M., Parrish W., and Hart M. (1988) Crystal structures of quartz and magnesium germanate by profile analysis of synchrotron-radiation high-resolution powder data. *J. Appl. Cryst.* **21**, 182–191.

Xu X., and Goddard W. A. I. (2004) Bonding properties of the water dimer: a comparative study of density functional theories. *J. Phys. Chem. A* **108**, 2305–2313.

Zeebe R. E. (2005) Stable boron isotope fractionation between dissolved $B(OH)_3$ and $B(OH)_4^-$. *Geochim. Cosmochim. Acta* **69**, 2753.

Zicovich-Wilson C. M., Pascale F., Roetti C., Saunders V. R., Orlando R., and Dovesi R. (2004) Calculation of the vibration frequencies of α-quartz: the effect of Hamiltonian and basic set. *J. Comput. Chem.* **25**, 1873–1881.

Associate editor: James Kubicki